PAM-Engineered Toehold Switches as Input-Responsive Activators of CRISPR-Cas12a for Sensing Applications

Neda Bagheri,[1] Alejandro Chamorro, [1] Andrea Idili,[1] Alessandro Porchetta,[1, #]

[1]Department of Sciences and Chemical Technologies, University of Rome, Tor Vergata, Via della Ricerca Scientifica 1, 00133, Rome, Italy.

ABSTRACT: The RNA-programmed CRISPR effector protein Cas12a has emerged as a powerful tool for gene editing and molecular diagnostics. However, additional bio-engineering strategies are required to achieve control over Cas12a activity. Here, we show that Toehold Switch DNA hairpins, presenting a rationally designed locked protospacer adjacent motif (PAM) in the loop, can be used to control Cas12a in response to molecular inputs. Reconfiguring the Toehold Switch DNA from a hairpin to a duplex conformation through a strand displacement reaction provides an effective means to modulate the accessibility of the PAM, thereby controlling the binding and cleavage activities of Cas12a. Through this approach, we showcase the potential to trigger downstream Cas12a activity by leveraging proximity-based strand displacement reactions in response to target binding. By utilizing the *trans*-cleavage activity of Cas12a as a signal transduction method, we demonstrate the versatility of our approach for sensing applications. Our system enables rapid, one-pot detection of IgG antibodies and small molecules with high sensitivity and specificity even within complex matrices. Besides the bioanalytical applications, the switchable PAM-engineered Toehold Switches serve as programmable tools capable of regulating Cas12a-based targeting and DNA processing in response to molecular inputs and hold promise for a wide array of biotechnological applications.

INTRODUCTION

CRISPR-associated (Cas) nucleases coupled to a guide RNA are sequence-dependent nucleic acid-targeting systems capable of recognizing and cleaving complementary nucleic acid sequences. [1-3] The programmability of CRISPR-Cas systems has allowed the development of revolutionary approaches in the field of nanobiotechnology, ranging from genome editing [4] to imaging [5] and *in vitro* diagnostics. [6-7] To fully harness their capabilities, it is crucial to implement strategies to improve the efficiency, specificity, and spatiotemporal regulation of CRISPR-Cas enzyme activities. [8] In this regard, a number of customized transcriptional, post-transcriptional/translational control strategies have been reported for the precise control of CRISPR-Cas biogenesis and interference mechanisms. [9-12] These also include the use of engineered guide RNAs (i.e. conditional gRNA) that can change their conformation in response to a molecular input (e.g., RNA sequence, small molecules [13-15]) to drive the activity of the CRISPR system to a specific target gene. This approach has allowed to achieve spatiotemporal control of gene expression in bacterial and mammalian cells. [16-17]

Recently, other strategies based on nucleic acid strand displacement reactions (SDRs) for controlling DNA-targeting CRISPR-based systems have been reported to work *in vitro* and *in vivo*. [8, 18-19] This reaction allows for reversible, sequence-controlled switching between single- and double-stranded DNA (dsDNA), as well as other nucleic acid secondary structures (e.g., hairpin, triplex, etc.). [20-21] The SDR takes advantage of the invasion of a DNA or RNA duplex structure by a third oligonucleotide, a process in which two strands anneal with each other displacing one pre-hybridized strand. Due to the predictability of Watson-Creek-Franklin base-pairing interactions, SDRs have been widely utilized for controlling complex reaction networks, [22-25] molecular computing, [21, 26] and nanostructured materials [27-30] and also serve as the foundation for a diverse range of biomolecular sensors. [31-34] Since reversible switching of nucleic acid structures between alternative conformations can be achieved through strand displacement reactions, this reaction can be easily integrated with CRISPR-based systems offering a valid bioengineering tool to facilitate the construction of artificial logic gates programmed to precisely and autonomously control gene expression in response to multiple inputs. [35-37]

SDR-based strategies have found applications also in CRISPR-based nucleic acid diagnostics. [38-39] In this regard, CRISPR systems controlled by SDRs have been reported in the context of CRISPR-Cas Type V or VI-based biosensing applications. [40-41] In these systems, the formation of a ribonucleoprotein (RNP) complex between the Cas enzyme and crRNA triggers both site-specific (*cis*-cleavage) and specific (*trans*-cleavage) nuclease activities, responsible for DNA/RNA reporter digestion and catalytic signal generation. While a single crRNA binds to the Cas nuclease and targets the nucleic acid of interest, switchable crRNAs responsive to target molecules have to be designed so that *trans*-cleavage is activated only upon target-binding induced reconfiguration. [6] However, the applicability of this approach is limited for sensing non-nucleic acid targets. It necessitates the design of customized ligand-regulated crRNAs that embed a recognition element (e.g., aptamers, ribozymes, etc.) in the crRNA sequence, thus imposing sequence constraints and restricting the generality of this sensing strategy. Other sensing approaches rely instead on the presence of a bio-transduction element (e.g., aptamer, DNAzyme, riboswitch) or more complex DNA circuits[42] converted into a functional activator of Cas proteins only upon target-induced reconfiguration [43-44].

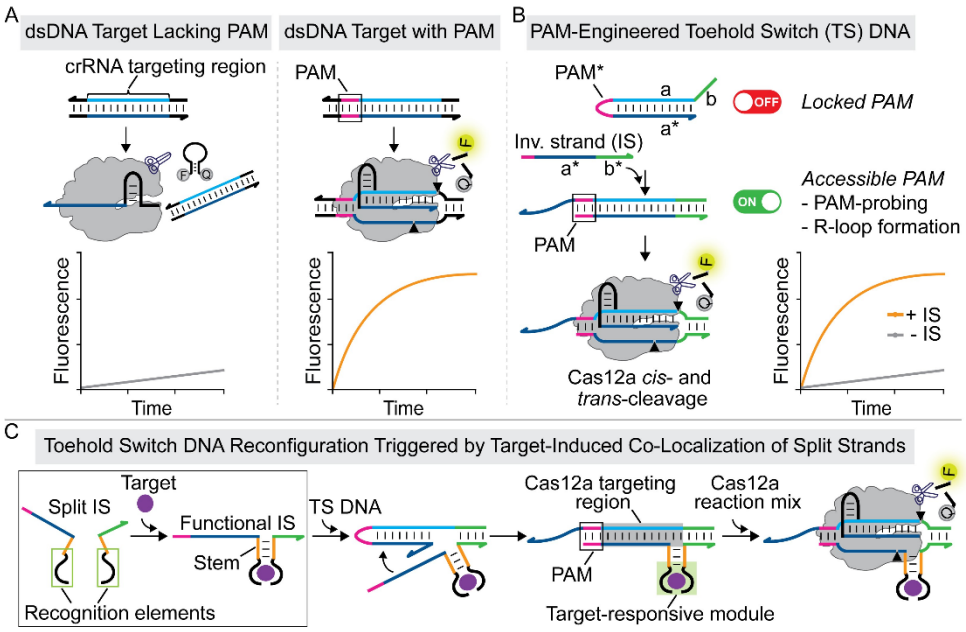

Figure 1. Switching on Cas12a activity using PAM-engineered toehold switch DNA. A) Representation of the PAM-dependent *cis*- and *trans*-cleavage activity of Cas12a. B) PAM-engineered Toehold Switch DNA provides a means to rationally control Cas12a activities through a toehold-mediated strand displacement reaction. The hairpin-to-duplex conformational switch can be easily associated with PAM complementation, leading to Cas12a binding and cleavage activity. C) The hairpin-to-duplex conformational switch can be further regulated by proximity-based reaction networks controlled by molecular inputs. The target-induced co-localization of two rationally designed split DNA strands leads to the formation of a functional invading strand (IS) that is able to induce reconfiguration of the toehold switch DNA. The PAM complementation is associated with Cas12a targeting and consequent cleavage activity. This mechanism can be easily generalized for the detection of any target molecule for which two recognition elements can be conjugated to a nucleic acid strand and it also allows spatially separate Cas12a targeting and the target-responsive module.

Despite expanding the set of detectable molecular inputs using CRISPR, these platforms face limitations due to sequence constraints of the functional element. Additionally, they often result in competitive assays, where the target molecule and crRNA compete for binding to the same functional nucleic acid. This usually leads to multi-step analyses, hindering translation into point-of-care diagnostic devices [45]

Inspired by the design of toehold switch RNA for molecular diagnostics, [46-48] here, we report on a strategy to control Cas12a activity using a rationally designed toehold switch DNA hairpin (TS DNA) presenting a locked protospacer adjacent motif (PAM) in the loop. Using strand displacement reactions to induce hairpin-to-duplex reconfiguration of TS DNA, we have successfully demonstrated the capability to control PAM accessibility to Cas12a binding in response to a molecular input and, consequently, regulate Cas12a activity. We also show that PAM-engineered TS DNA can be rationally controlled by a proximity-based reaction network to achieve Cas12a-powered single-step detection of miRNAs, antibodies, and small molecules. The proposed approach results in a programmable universal CRISPR sensing platform that supports the rapid, one-pot detection of any target molecule for which a specific recognition element can be conjugated to a DNA strand.

RESULTS AND DISCUSSION

Switching on Cas12a activity through PAM-engineered toehold switch DNA.

Successful CRISPR-based targeting requires two factors such as complementarity between the guide RNA and the nucleic acid target, and a short PAM flanking the target. The DNA-targeting Cas nucleases (e.g., Cas9, Cas12a) scan available DNA for a PAM before probing guide-target complementarity. By doing so, the PAM plays an essential role in the CRISPR-based adaptive immune system of bacteria and archaea since it serves as a gatekeeper preventing the enzyme from targeting DNA sequences encoded in the CRISPR array. [49-50]

From a sensing perspective, however, this aspect poses a significant limitation because it restricts our ability to target any dsDNA sequence. To date, only a few ingeniously PAM-free detection strategies for both nucleic [51-52] and non-nucleic acid [53] targets have been reported. However, despite extensive efforts in engineering Cas enzymes with relaxed or altered PAM requirements, [54] the limitation of specific PAM sequences is still shared by most CRISPR nucleases and is essential for both cis- [55] and trans-cleavage of Cas12a in the presence of dsDNA targets (Figure 1A). [56]

Here we take advantage of PAM constraints to rationally design toehold switch DNA hairpins (i.e., PAM-engineered Toehold Switches) triggering CRISPR-Cas12 activity only in response to an external input molecule. Specifically, we re-engineered Cas12-targeting dsDNA introducing a hairpin-to-duplex conformational switch. We achieve this by simply sequestering the anti-PAM (PAM*) sequence within a short loop that connects the two Cas12a-targeted self-complementary portions (Figure 1B). In our design, PAM-engineered Toehold Switches display a PAM sequence that is not complemented as an anti-PAM (PAM*) is sequestered in

a “locked” state, making the hairpin unable to trigger cleavage activities.

.

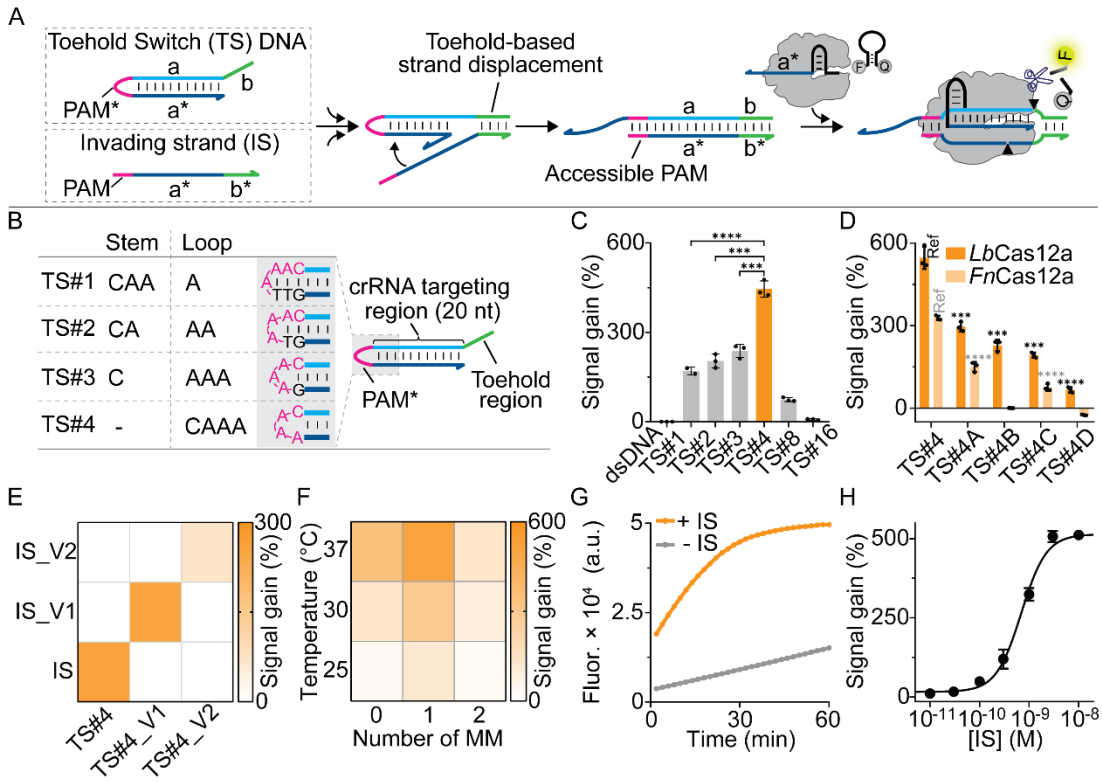

Figure 2. Design and optimization of PAM-engineered toehold switch DNA triggering Cas12a *trans*-cleavage activity upon strand displacement reaction. A) Schematic representation of the hairpin-to-duplex reconfiguration and PAM complementation controlled by a strand displacement reaction of toehold switch DNA, leading to the activation of Cas12a *trans*-cleavage. B) Design of toehold switch (TS) DNA with varying numbers of bases (PAM*) concealed within the loop. C) Measurement of the *trans*-cleavage activity of Cas12a, represented as fluorescence signal gain, upon strand displacement using different TS DNA sequences, both in the absence and presence of the complementary invading strand (5 nM). D) Signal gain analysis of TS#4 variants (1 nM) in the presence (5 nM) and absence of the invading strand (IS) using different Cas12a orthologs in the reaction mix. E) Plot illustrating the sequence-dependent and highly specific *trans*-cleavage signal gain of TS DNA sequences with different Cas12a-targeting domains. Activation occurs only in the presence of a complementary invading strand (5 nM). F) Impact of temperature and number of mismatches in the CRISPR-targeting domain (a*) on the overall signal gain associated with *trans*-cleavage of TS DNA upon the strand displacement reaction ([IS] = 5 nM). G) Fluorescence kinetic analysis over time, showcasing the regulation of *Lb*Cas12a *trans*-cleavage activity by TS#4 with and without a fully complementary invading strand (5 nM). H) Dose-response curve demonstrating the response to strand displacement by increasing concentrations of the invading strand (IS) (t = 15 min) using a fixed amount of TS#4 (1 nM). The experiments were conducted at 37 °C by adding Cas12a reaction mix (500 nM of FRET-based DNA reporter and 20 nM of Cas12a/crRNA) to the buffer solution containing Toehold Switch DNA (1nM) and a specific concentration of invading strand. Signal gain (%) values were calculated after 15 min cleavage reaction. It represents the relative fluorescence signal change associated with *trans*-cleavage activity achieved upon the addition of the invading strand relative to the background fluorescence obtained in its absence. Error bars represent the deviation from three independent experiments. Two-tailed unpaired Student’s t-test was performed to analyze statistical differences between the two comparisons and the p-value ranges are indicated with asterisks (****P ≤ 0.0001; ***P ≤ 0.001; **< P ≤ 0.01; *P ≤ 0.05). Asterisks in (C) indicate comparisons to TS#4. Black and gray asterisks in (D) indicate comparisons to the corresponding colored “Ref”.

To induce the hairpin-to-duplex conformational switch and consequent PAM complementation, we used a toehold-mediated strand displacement reaction.[20] As a proof of concept demonstration, a functional Invading Strand (IS) can be a single stranded target (DNA or RNA) designed to be the non target strand (NTS, “a*” portion in Figure 1B and C) complementary to the target strand (TS) sequestered in the stem of the hairpin (“a” portion, light blue). Of note, the SDR reaction can be activated only through the introduction of a short sequence called toehold (“b” portion, green) which triggers the strand displacement reaction between the hairpin structure and the IS.

In addition, to extend the classes of molecular targets that can control our switchable Cas12a-based system, we re-engineered the functional IS to be responsive to non-nucleic acid targets (Figure 1C). To do so, we split the functional IS into two separate portions (i.e., Split IS), each one terminally modified with a specific recognition element. The idea is that the simultaneous binding of the target molecule to the two recognition elements can induce their co-localization, bringing the two split units into close proximity.[57-59] The two Split IS can be rationally designed in a way that the hybridization of their short complementary portions

(orange motifs, Figure 1B) leads to the formation of a restored functional Invading Strand (IS) only upon target binding (purple sphere, Figure 1C). The co-localization-induced reconstitution of the functional IS can be used to activate the hairpin-to-duplex reconfiguration through a toehold-mediated SDR. This manipulation enables the PAM to become accessible for Cas12a binding, thereby activating both the *cis*- and *trans*-cleavage activities of Cas12a in response to external molecular inputs. Of note, in our design, the target-responsive module (green region, Figure 1C) does not directly interact with the Cas12a-targeting region (grey region) in the presence of the target. This provides a means to turn on Cas12a activity in response to any external input without the need for direct matching between the guide RNA and the molecular target. The input-responsive and the Cas12a-targeting modules are indeed spatially separated, allowing for independent target binding and activation of Cas12a cleavage activities.

Design and Optimization of PAM-Engineered Toehold Switch DNA for Enhanced Trans-Cleavage via Strand Displacement Reaction

A PAM-engineered Toehold Switch DNA (TS DNA) is composed of three major domains: 1) a single stranded loop (Figure 2A, pink loop) functioning as a sequence domain complementary to the PAM (e.g., 5'-TTTV-); 2) two self-complementary DNA motifs (e.g. "a/a*", blue region in Figure 2A) that represent the crRNA targeting portion; 3) a 3'- terminal toehold ("b", green portion) necessary for the strand displacement reaction. To ensure that the hairpin switch triggers Cas12a activity only upon a toehold-mediated SDR and PAM complementation, we characterized the activation of TS DNAs using single stranded DNA inputs as invading strands (IS). As our test bed, we monitored the *trans*-cleavage activity of Cas12a in the absence and in the presence of IS using an external FRET-based stem-loop DNA probe as a reporter of fluorescence. [60]

Specifically, we designed a set of TS DNAs sharing the same 20 nt long crRNA targeting portion ("a/a*", the blue region in Figure 2A) and the same toehold region ("b", the green motif in Figure 2A) but a different number of nucleotides in the loop. C

onsidering that optimal PAM of Cas12a consists of four nucleotides at the 5' in the non-target strand (i.e., NTS, 5'-TTTV-), we designed a set of TS DNA variants having a variable loop length comprised between 1 to 16 nt of anti-PAM bases (i.e., PAM*) hidden in the loop (Figure 2B). All the TS DNAs act as switching regulators of Cas12a, exhibiting a measurable change of the fluorescent emission associated with enhanced trans-cleavage activity upon the addition of the IS (5 nM, Figure 2C). This confirm that the hairpin-to-duplex structure switching and PAM complementation can be monitored as a means of fluorescence signal change due to different trans-cleavage between the hairpin and duplex states (see also Materials and Methods section). Notably, we observed that by increasing the number of PAM* nucleotides hidden in the loop from 1 nt to 4 nt significantly reduces the fluorescence background generated by the TS DNA (Figure S1). In the presence of an invading strand, however, all TS DNAs switch to the same double stranded DNA, resulting in identical trans-cleavage activity and fluorescence output. Consequently, TS#4 displays the highest signal gain upon IS addition (5 nM) compared to the other toehold switches (1 nM). In contrast, increasing the number of PAM* nucleotides trapped in the loop (TS#8 and TS#16, Figure S1) leads to a significant fluorescence background, and the relative signal gain decreases (Figure 2C). This can be attributed to the lower thermodynamic stability (ΔGTS#8 = -13.42 kcal/mol, ΔGTS#16 = -13.52 kcal/mol) compared to the TS#4 (ΔGTS#4 = -14.32 kcal/mol) resulting in facilitated DNA-RNA heteroduplex formation even in the absence of the target IS. In contrast, TS#4 has a lower thermodynamic stability (ΔGTS#4 = -14.32 kcal/mol) compared to the other TS DNA variants presenting 1, 2, and 3 additional base pairing in the stem, respectively (ΔGTS#1 = -16.54 kcal/mol, ΔGTS#2 = -16.25 kcal/mol, ΔGTS#3 = -15.25 kcal/mol).

As a matter of fact, the slightly higher fluorescence background associated with TS#1, TS#2, and TS#3 in the absence of IS can not be ascribed to a facilitated hybridization with the crRNA.

It is noteworthy, however, that all the TS Switch shows a concentration-dependent signal background. As an example, the TS#4 concentrations required for significant collateral cleavage are substantially higher than those reported for dsDNA targets with accessible PAM motifs (LOD ~100 pM, Figure S2). This suggests that at a significantly higher concentration of TS#4, the targeting process is driven by the crRNA-DNA hybridization process, highlighting the importance of the RNA-DNA heteroduplex formation for stable Cas12a RNP binding. To minimize the signal background and maximize the signal gain we set the optimal concentration of TS#4 at 1 nM (Figure S3). Furthermore, as an additional control experiment, we tested a dsDNA with the same stem and toehold regions but a fully complemented PAM. As expected, the same fluorescence intensity before and after SDR was obtained. Overall, our data show an enhanced fluorescence signal change of TS#4 upon target-induced strand displacement (Figure 2C). Of note, the signal gain is also a function of the toehold length of IS and the number of the 5'-terminal overhanging nucleotides in the invading portion. Firstly, we tested TS DNAs with different lengths of toehold (from 0 nt to 18 nt, Figure S4). As expected, we observe an increase in the signal gain with the toehold length with a maximum signal change using a toehold longer than 6 nt. A similar trend is observed for the 5'-terminal overhanging nucleotides in the invading portion of the IS (from 0 to 8 nt, Figure S5). The presence of extra bases helps overcome the energetic barrier present in the unimolecular hairpin structure and allows quantitative hairpin-to-duplex conformational change in agreement with the thermodynamics of hairpin strand displacement reactions. [20]

To demonstrate the generalizability of our approach, we also tested our TS DNA using different Cas12a orthologs. Indeed, Cas12a exhibits widely different *trans*-cleavage activity between related orthologs and altered PAM specificities. [61] To study this, we designed mutated TS#4 having non canonical PAM* sequences

hidden in the loop and tested them using different Cas12a orthologs, as from the *Francisella novicida* (*Fn*Cas12a) and the *Lachnospiraceae bacterium* (*Lb*Cas12a) (Figure 2D). We found that also TS#4 DNA variants having suboptimal G-containing PAM* (i.e., C-containing PAM in the invading strand) turn on *trans*-cleavage in the presence of the IS using either *Lb*Cas12a or *Fn*Cas12a. As expected, the TS#4 variant leads to the highest increase in fluorescence output, according to the fact that the PAM-complemented duplex contains the optimal PAM (i.e., 5'-TTTV) for *trans*-cleavage of Cas12a. [54, 61] Then, we focused on the design of the CRISPR-targeting region of the hairpin switch. We selected a 20 nt long stem of the hairpin ("a/a*") because this is widely reported as the optimal length of dsDNA targets for the generation of maximum *trans*-cleavage activity in Cas12a systems. [62] However, it is well established that the *trans*-cleavage of Cas12a is also dependent on the specific crRNA sequence. [62-63] Thus, we designed and tested a set of TS#4 DNAs having different crRNA-targeting sequences by using corresponding IS counterparts. The signal gain observed clearly confirms that our strategy can be adapted for any CRISPR-targeting sequence, and the *trans*-cleavage is switched on in a highly specific way only in the presence of the complementary IS (Figure 2E and S6).

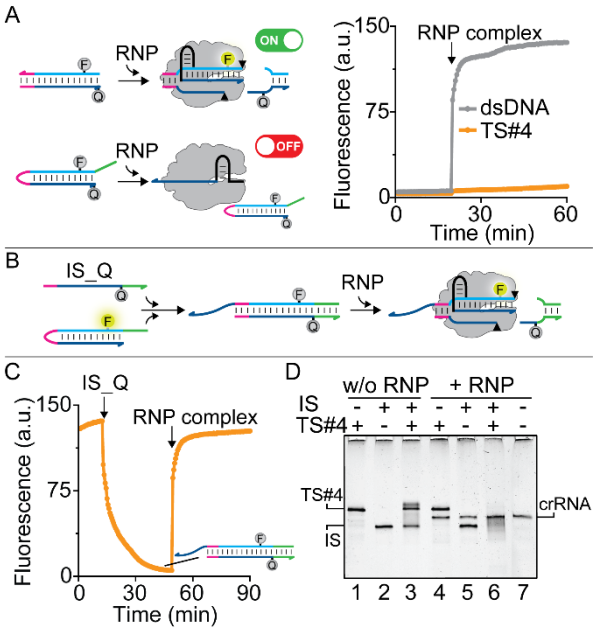

Figure 3. *Cis*-cleavage activity of Cas12a in response to hairpin-to-duplex reconfiguration. A) Time-course fluorescence experiments of cis-cleavage activities using FRET-labelled double-stranded and toehold switch DNA having the same Cas12a-targeting portion (a/a*). By adding pre-hybridized the RNP complex (final concentration of 20 nM), the dsDNA (10 nM) in solution was cleaved but not the toehold switch (i.e., TS#4_F-Q, 10 nM). B) Schematic description of the strand displacement reaction using FAM-labelled hairpin DNA (i.e., TS#4_F) and BHQ1-labelled invading strand (i.e., IS_Q). C) Time-course fluorescence assay of the hairpin-to-duplex reconfiguration induced by SDR (i.e., [IS] = 10 nM). By adding IS_BHQ1 (10 nM) to a fixed amount of TS#4_F (10 nM) a rapid quenching of fluorescence represents the SDR associated with hairpin-to-duplex switch and PAM complementation. Upon the addition of the RNP complex (final concentration of 20 nM) a rapid increase to the original fluorescence value is associated with quantitative *cis*-cleavage activity of the reconfigured TS#4. D) Denaturing PAGE analysis of the *cis*-cleavage activity of Cas12a (37 °C, reaction time of 5 min) on toehold switch DNA (i.e., TS#4) showing degradation of TS#4 in the presence of invading strand (Lane 6) but not in its absence (Lane 4). Here the fluorescence experiments were performed at 37 °C in a 45 µL buffer solution and the fluorescence was measured using FAM emission according to the experimental procedures reported in the Supporting Information.

Finally, we optimized the TS DNA by studying the effects of mismatches (i.e., MM) in the CRISPR-targeting region (0, 1, and 2 mismatches in the "a*" region) and the temperature of the assay (from 25 °C to 37 °C, Figure 2F). We achieved the highest signal change at the temperature of 37 °C using TS#4, which contains one mismatch in the middle of the a* region (C-A mismatch). Under such experimental conditions, our system responds rapidly to the addition of IS, generating a rapid increase in the fluorescence signal at saturating concentration of IS (3 nM; Figure 2G) and a sensitivity comparable to the one reported for pre-amplification-free Cas12a-based detection platforms ($k_{1/2}$= 0.5 ± 0.1 nM, LOD= 8.9 pM, Figure 2H).

Characterization of *cis*-cleavage activity of Cas12a using PAM-engineered Toehold Switch DNA.

To better investigate how the hairpin-to-duplex switching mechanism regulates the Cas12a activity, we also characterized the system monitoring the *cis*-cleavage activity. Generally, the *cis*-cleavage of dsDNA targets is a result of PAM-dependent DNA duplex unwinding, electrostatic stabilization of the displaced non target DNA strand (NTS), and sequential cleavage of the NTS and target DNA strands. [64] Since cleavage by LbCas12a occurs at ~17 bases 3' of the PAM and leaves 5' overhanging ends by releasing the PAM-distal DNA cleavage product, we performed fluorescence and denaturing gel electrophoresis assays using the optimized toehold switch sequence (TS#4) modified with an internal FAM and a 3'- terminal BHQ1 (i.e., TS#4_F-Q). Firstly, we monitored the fluorescence signal change over time of TS#4_F-Q (10 nM). By adding a fixed amount of Cas12a/crRNA complex (20 nM), no significant change of fluorescence is observed, indicating that *cis*-cleavage can not be efficiently activated unless PAM is fully complemented (Figure 3A). On the contrary, a standard dsDNA with fully complemented PAM rapidly generates a *cis*-cleavage associated signal output. Next, we monitored *cis*-cleavage activation upon strand displacement reaction using a FAM-labelled TS#4 (i.e., TS#4_F) and an invading strand containing an internal BHQ1 quencher (i.e., IS_BHQ1). By sequentially adding the IS_BHQ1 (10 nM) and the RNP complex (final concentration of 20 nM), an initial quenching of the fluorescence is observed because of the hairpin-to-duplex structural change followed by a rapid increase of fluorescence due to *cis*-cleavage activity associated to the release of PAM-distal DNA cleavage product (Figure 3B and C). This concept was further confirmed by denaturing polyacrylamide gel electrophoresis (PAGE) assay (Figure 3D). Indeed, TS#4 was not digested either in the presence and in the absence of RNP, but cleavage occurs only upon pre-incubation with the IS, confirming the need for SDR and

PAM complementation to trigger the Cas12a-based system.

Cas12a-powered sensing platforms based on target-induced split hybridization network and Toehold Switch DNA.

We characterized the second strategy based on the co-localization of split input strands onto the same target to achieve reconfiguration of TS DNA through SDR. This approach, previously reported for controlling strand displacement reactions and cascades, [27, 59, 65-66] draws inspiration from previous protein-based complementation assays, [67-68] and nucleic acid-based systems for biosensing.[59, 69] To evaluate the possibility of using co-localization of split invading strands to control the hairpin strand displacement reaction, we first studied our system using a single stranded DNA designed to emulate the target-induced co-localization of split-invading strands.

The Split Mimic effectively simulates the co-localization of two split strands through target binding, featuring an intramolecular stem-forming region (6 nt) and two flanking portions complementary to the toehold and invading portions, respectively. This intramolecular stem brings the two flanking portions into close proximity to each other, mimicking the co-localization induced by the binding of a target antibody and creating a structure resembling a conventional linear invading strand. Kinetics experiments of trans-cleavage clearly indicate that the bulge created by the stem in the Split Mimic does not significantly reduce the overall efficiency of strand displacement and allows efficient hairpin-to-duplex reconfiguration of TS#4 in a concentration-dependent fashion (Figure S7).

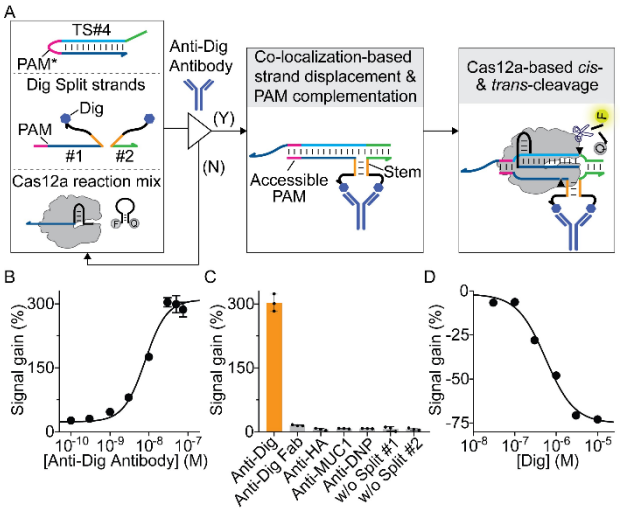

Figure 4. Cas12a-powered anti-Dig antibody detection using PAM-engineered toehold switch DNA. A) General scheme depicting our sensing strategy for the detection of anti-Dig antibodies. Co-localization of Dig-modified split invading strands (Dig-Split #1 and #2) induced by the antibody target leads to the hairpin-to-duplex reconfiguration of the toehold switch DNA (TS#4), followed by PAM complementation and activation of Cas12a *trans*-cleavage, resulting in the generation of a fluorescence output. B) Plot of signal gain (%) as a function of anti-Dig antibody concentration ($K_{1/2}$ = 7.9 ± 0.8 nM, LOD = 20 ± 5 pM). C) Determination of the specificity of the Cas12a-powered platform comparing anti-Dig antibody with negative controls (i.e., 100 nM). D) Detection of free digoxigenin in solution using a competitive format of the Cas12a-based assay for anti-Dig antibody detection. Here a fixed amount of anti-Dig antibody (30 nM) is pre-incubated with equimolar concentration of Dig split #1 and #2 (30 nM), and different concentrations of digoxigenin are added in solution before the addition of the Cas12a reaction mix for the generation of the output ($K_{1/2}$ = 0.55 ± 0.01 µM, LOD = 13 µM). The experiments were conducted at 37 °C in 45 µL buffer solution containing 1 nM of TS#4, equimolar concentrations of Dig Split strands (30 nM), and a specific concentration of anti-Dig antibody by adding Cas12a reaction mix (500 nM of FRET-based DNA reporter and 20 nM of Cas12a/crRNA complex). Error bars represent the deviation from three independent experiments.

Then, we aimed to provide proof of the principle of TS DNA reconfiguration and subsequent Cas12a *trans*-cleavage activation controlled by the binding of a target analyte. Essential to the split sensing system is the requirement for a target molecule capable of inducing the co-localization of two split DNA strands to reconstitute a functional Invading Strand. To demonstrate this concept, we utilized the miR-21 target as a model target molecule. Thus, we have split the Split Mimic into two separated miR21-targeting Split Strands. The first one has a 12-nt toehold-binding DNA strand (i.e., miR-21 Split#1), and the second one with a fully complementary invading domain (i.e., miR-21 Split#2, Figure S8A). Both sequences were then flanked by two miR21-targeting DNA sequences (11 nt long) at their 5'- and 3'- ends, respectively. By adding increasing concentrations of the miR-21 target in a solution containing all the components of the split hybridization network, *trans*-cleavage of Cas12a is switched on and an amplified fluorescence output is obtained with a concentration-dependent profile. This results in a rapid, single-step, and specific miR-21 detection ($k_{1/2}$= 7.2 ± 1.2 nM, LOD= 150 pM, Figure S8B-D).

While a pre-amplification step is essential for achieving sufficient sensitivity in miRNA detection, our study serves as a proof-of-principle demonstration for detecting any single-stranded DNA/RNA sequence. Notably, this approach eliminates constraints related to PAM sequences and eliminates the need to alter the crRNA sequence based on the specific target sequence.

Turning on CRISPR-Cas12a cleavage activity using antibody-controlled toehold switch DNA.

Motivated by the above results, we tested our system using IgG antibodies as target molecules. All IgG antibodies present a specific Y-shaped geometry and two identical binding sites separated by about 8-14 nm which make them ideal substrates for co-localization-based sensing platforms. [70-72] Our hypothesis is that IgG antibody binding to the two antigen-conjugated split input strands triggers their simultaneous co-localization on the same scaffold antibody, thus increasing the local effective molarity of Dig Split Strands. This leads to the reconstitution of a functional invading strand complex, activating the strand displacement reaction and subsequent hairpin-to-duplex reconfiguration of PAM-engineered TS#4, resulting in signal generation (Figure 4A)

To demonstrate our hypothesis, we initially used the small molecule digoxigenin (Dig) as the recognition element and an anti-Dig IgG antibody (i.e., anti-Dig Ab) as the target analyte. We have split the DNA invading

strand into two separate Dig Split Strands. The first one has a 12-nt toehold-binding DNA strand (Dig Split #1, green portions in Figure 4A), and the second one has a fully complementary invading domain (Dig Split #2, blue and pink portions). Both sequences were then flanked by two short complementary stem-forming domains (orange portions) and by two poly-thymine tails presenting the recognition element (i.e., Dig antigen) at their 5'- and 3'- ends. To optimize antibody detection, we tested various lengths of the stem-forming domain between Dig Split#1 and #2. Our goal was to identify the optimal stem-forming domain, ensuring no strand displacement reaction occurs in the absence of anti-Dig antibodies, while achieving the highest signal change in their presence. We find that a 6-nt forming stem leads to the strongest difference in efficiency between the absence and presence of a fixed concentration of anti-Dig antibody (100 nM, Figure S9).. To further optimize the CRISPR-based assay, we also selected the optimal concentrations of Dig Split #1 and #2 (30 Nm, Figure S10) and pH (Figure S11). Under such optimal experimental conditions, our CRISPR-based detection responds quantitatively, generating a 4-fold increase in fluorescence at saturating concentration of anti-Dig antibodies within 30 min and achieving sensitivity in the picomolar range (LOD = 190 pM, $K_{1/2}$ = 7.9 ± 0.8 nM Figure 4B and S12). The platform is also highly specific because the fluorescence is generated by the binding of the anti-Dig antibody to the two recognition elements and no significant signal change is observed in the presence of nonspecific antibodies (Figure 4C). In addition, the system can also be easily converted to detect free antigens (i.e., Dig) in a single-step competitive assay (Figure 4D). Notably, the platform is capable of detecting anti-Dig antibodies also in blood serum (from 20 to 50 %) without significant changes in LOD and specificity (Figure S13).

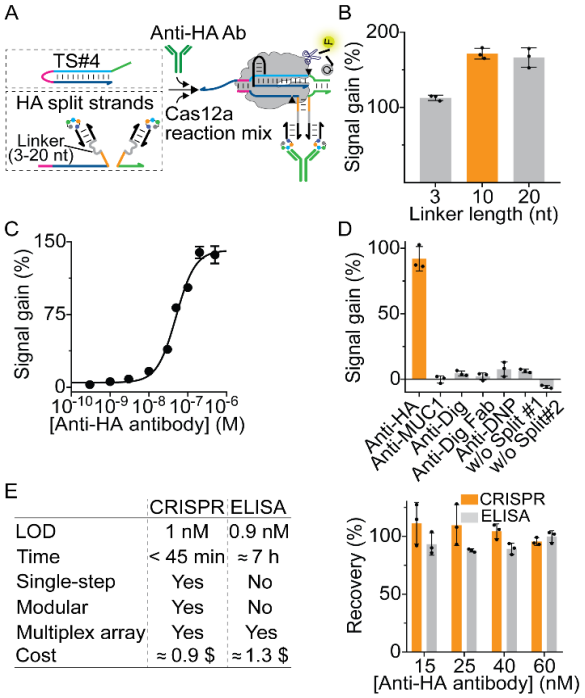

Figure 5. Modular Cas12a-powered platform for the detection of anti-HA antibodies. A) Modular design employing a peptide-PNA chimera probe (HA-PNA) pre-hybridized to HA Split Strands (i.e. HA_Split#1_L#10 and HA_Split#2_L#10) to detect Anti-HA antibodies. B) Plot showing fluorescence signal gain (%) obtained for anti-HA antibody detection at 200 nM concentration using HA split strands having different linker lengths. C) Binding assay using increasing concentration of anti-HA antibodies ($K_{1/2}$ = 50 ± 3 nM; LOD = 1 nM). D) Specificity test of the detection platform using non specific target antibodies (i.e., 100 nM) and different control experiments. E) Comparision of our CRISPR-based assay with ELISA for anti-HA antibody detection. The fluorescence experiments were conducted at 37 °C in a 25 µL solution containing 1 nM of TS#4, an equimolar concentration of HA Split strands (HA_Split#1_L#10 and HA_Split#2_L#10, 10 nM), peptide-PNA chimera probe (HA_PNA_9, 20 nM) by adding a specific concentration of anti-HA antibody and the Cas12a reaction mix. Recovery test experiments were performed in 10% serum samples spiked at different concentrations of anti-HA antibodies according to the experimental procedures reported in the Supporting Information. Error bars represent the deviation from three independent experiments.

Our sensing mechanism is highly versatile, as it allows for the detection of various classes of target antibodies and antigens by simply changing the recognition elements conjugated to the oligonucleotide. To demonstrate this, we decided to explore more complex antigens-antibody pairs. Peptides are widely recognized as representative antigens for diagnostic antibodies. However, attaching peptides to DNA sequences presents challenges in terms of cost and synthesis, which could hinder the practical use of our platform for diagnostics. Considering these factors, we have developed a modular version of our platform that requires a total of three oligonucleotides, with only one of them labeled with the specific peptide. Using this new set of sequences, the peptide-conjugated strand serves as a scaffold to bind both the DNA Split Strands (Figure 5A). To facilitate the conjugation of peptides, we employed peptide-nucleic acid (PNA) as the antigen-conjugated strand. PNA is a DNA mimic with a pseudopeptide backbone that maintains high sequence specificity toward DNA complementary strands, simplifying the conjugation process. [73-74]

In our new modular and versatile approach, we used a 9-residue HA epitope (HA) present in the hemagglutinin (HA) protein on the surface of influenza viruses as the recognition element for the detection of anti-HA antibodies (Figure 5A). Influenza outbreaks exert a significant impact on society, encompassing mortality rates and economic ramifications. Therefore, it is crucial to carry out clinical evaluations of influenza viral diseases and closely monitor immune responses to influenza vaccines or infections. To optimize the detection system, we further refined the molecular design. Our emphasis was on investigating different lengths of the DNA portion between the stem-forming domain and the complementary portion to PNA (referred to as the Linker in Figure 5A) of HA split strands. Extending the linker from 3 to 10 nucleotides resulted in a higher signal gain (HA_Split#1_L#10 and HA_Split#2_L#10, Figure 5B), likely due to enhanced system flexibility. We also explored different PNA lengths (9 and 17 nucleotides) to assess the potential impact of the length of the hybrid PNA-DNA duplex on the binding to the target antibody utilized (HA-PNA_9, Figure S14) and determined the optimal concentration of HA split strands (Figure S15).[75] Our single-step

CRISPR platform for anti-HA Ab detection demonstrated good sensitivity (Figure 5C and Figure S16) and specificity (Figure 5D, K1/2 = 50 ± 3 nM; LOD = 1 nM). We then applied our system for the detection of anti-HA antibodies in blood serum (10%). Statistical analysis revealed a linear range between 5 and 70 nM anti-HA antibody with R2 =0.93, reaching a plateau at approximately at 100 nM of anti-HA antibody (Figure S17) in 10% serum sample. To benchmark our assay with the gold standard ELISA assay (Figure S18) and validate our method, we conducted a spike and recovery assessment through quantification of anti-HA antibody with ELISA and CRISPR-based assay in blood serum. Specifically, spiked sera (10% v/v dilution) were prepared to achieve four standard concentrations (15, 25, 40, 60 nM, Figure 5E). Our CRISPR-based platform successfully identified these concentrations with optimal recoveries ranging from 95% to 111%. The CRISPR platform demonstrated comparable sensitivity (see table in Figure 5E) and significant potential for single-step detection of specific antibodies in a shorter analysis time compared to ELISA (approximately 7 hours), following a relatively simple sample preparation (30 minutes of pre-incubation between Cas12a/crRNA).

In addition, another 15-residue MUC1-epitope (MUC1) for the recognition of the anti-MUC1 antibody has been conjugated to the same PNA strand (i.e., MUC1-PNA, Figure S19). By doing so, we aim to show the potential applications of our approach for the rapid, single-step detection of circulating anti-MUC1 antibody levels in blood serum.[76] Also, this second modular CRISPR platform exhibited comparable sensitivity ($K_{1/2}$ anti-MUC1= 5.1 ± 0.9 nM, LOD = 95 pM), reproducibility, and high specificity compared to the non-modular version described earlier. The sensors also demonstrated similar LOD and specificity, indicating that the larger antigens and the presence of PNA did not significantly affect the Cas12a-based detection platform.

CONCLUSION

Our study presents the rational design of PAM-engineered toehold switch DNA hairpins as target-responsive activators of CRISPR-Cas12a. Specifically, we demonstrate that is possible to switch on Cas12a activity as a means of hairpin-to-duplex structure switching and PAM complementation. By combining co-localization-based DNA hybridization networks with hairpin strand displacement reactions we turn on Cas12a-based cleavage activities in response to the binding of different molecular inputs. By taking advantage of Cas12a *trans*-cleavage, we report on the sensitive detection of different analytes, such as miR-21, two clinically relevant IgG antibodies (anti-MUC1 and anti-HA Ab), and small molecules (digoxigenin). Our sensing approach combines the signal amplification due to Cas12a multiple turnover *trans*-cleavage activity with the benefits of target-binding induced split complementation assays, enabling a streamlined, single-step measurement process also in complex matrices (blood serum) in a one-pot assay. As a result, our methodology is highly sensitive and specific, and exhibits a broad spectrum of applicability, as it is modular and can be easily adapted to the detection of any antibody, antigen and bivalent macromolecular targets provided that the relevant recognition element can be coupled to a nucleic acid strand. The CRISPR method also offers the possibility of array multiplexing at a cost of about $0.9 /sample, which is already comparable to that of ELISA assays ($1.3/sample estimated on anti-HA antibody platform). This potential, in turn, unveils novel prospects within the realms of molecular diagnostics and CRISPR-based point-of-care (POC) applications.

We also note other advantages compared to previously reported complementation-based assays. First, the fluorescence signal is not generated by complementation of split reporters (e.g., split fluorescent proteins, split luciferase, etc.) upon target binding. The RNP complex is already present in the solution but it is inactive as its natural substrate (i.e., PAM-accessible duplex DNA) is sequestered in a non-binding hairpin state. This may represent an overall advantage as target-induced re-assembly of split reporters generally presents some criticisms, such as spontaneous re-assembly, slow fluorescence generation, and lower catalytic activity of split enzymes compared to the corresponding full-sized protein. Indeed, our platforms for antibody detection shows high sensitivity with a LOD (low nM/high pM) that is approximately one order of magnitude lower than our previously reported studies using affinity-based proximity assays.[70, 77]

Besides the bioanalytical applications, our molecular strategy is versatile and it can be further adapted to other PAM-dependent Cas enzymes. We envision that the decoupling of the crRNA-targeting module responsible for enzyme activation from the target-responsive region may be of interest also for the rational design of novel conditional CRISPR systems, providing additional control on CRISPR-based targeting and downstream cleavage processing. These findings resonate with profound relevance, extending not only to the expansive community engaged in CRISPR-based biosensing but also captivating the attention of researchers immersed in synthetic biology, bioengineering, and nanomedicine.

ASSOCIATED CONTENT

The Supporting Information is available free of charge and contains *trans*-cleavage assays of *Lb*Cas12a upon strand displacement reactions, the optimization of the TS#4, as well as kinetics assays using IS, miR-21, and antibodies in buffer and in serum samples.

AUTHOR INFORMATION

Corresponding Authors

*alessandro.porchetta@uniroma2.it

Author Contributions

All authors have given approval to the final version of the manuscript. NB conducted the experiments and contributed to the manuscript. AC conducted the ELISA experiments. AI contributed to the scientific discussion and to the writing of the manuscript. AP conceived the idea for the study, wrote the draft, and supervised all the research activities.

Notes

The authors declare no competing financial interest.

ACKNOWLEDGMENT

The research leading to these results has received funding from AIRC under MFAG 2022 - ID. 27151 project – P.I. Porchetta Alessandro. A.P. acknowledge funding from the Italian Ministry of University and Research (Project of National Interest, PRIN, 2022FPYZ2N) We would like to thank the Nano-ImmunoEra project. Nano-ImmunoEra project has received funding from the European Union's MSCA Staff Exchange Horizon Europe programe Grant Agreement Number 101086341.

References

[1] K. S. Makarova, D. H. Haft, R. Barrangou, S. J. Brouns, E. Charpentier, P. Horvath, S. Moineau, F. J. Mojica, Y. I. Wolf, A. F. Yakunin, J. van der Oost, E. V. Koonin, *Nat. Rev. Microbiol.* **2011**, *9*, 467-477.

[2] J. Van Der Oost, E. R. Westra, R. N. Jackson, B. Wiedenheft, *Nat. Rev. Microbiol.* **2014**, *12*, 479-492.

[3] F. Jiang, J. A. Doudna, *Annu. Rev. Biophys.* **2017**, *46*, 505-529.

[4] J. A. Doudna, E. Charpentier, *Science* **2014**, *346*, 1258096.

[5] H. Wang, M. Nakamura, T. R. Abbott, D. Zhao, K. Luo, C. Yu, C. M. Nguyen, A. Lo, T. P. Daley, M. La Russa, Y. Liu, L. S. Qi, *Science* **2019**, *365*, 1301-1305.

[6] Y. Tang, L. Gao, W. Feng, C. Guo, Q. Yang, F. Li, X. C. Le, *Chem. Soc. Rev.* **2021**, *50*, 11844-11869.

[7] M. M. Kaminski, O. O. Abudayyeh, J. S. Gootenberg, F. Zhang, J. J. Collins, *Nat. Biomed. Eng.* **2021**, *5*, 643-656.

[8] H. Shivram, B. F. Cress, G. J. Knott, J. A. Doudna, *Nat. Chem. Biol.* **2021**, *17*, 10-19.

[9] H. R. Kempton, L. E. Goudy, K. S. Love, L. S. Qi, *Mol. Cell* **2020**, *78*, 184-191. e183.

[10] N. D. Marino, R. Pinilla-Redondo, B. Csörgő, J. Bondy-Denomy, *Nat. Methods* **2020**, *17*, 471-479.

[11] L. R. Polstein, C. A. Gersbach, *Nat. Chem. Biol.* **2015**, *11*, 198-200.

[12] D. Manna, B. Maji, S. A. Gangopadhyay, K. J. Cox, Q. Zhou, B. K. Law, R. Mazitschek, A. Choudhary, *Angew. Chem. Int. Ed.* **2019**, *131*, 6351-6355.

[13] S. P. Collins, W. Rostain, C. Liao, C. L. Beisel, *Nucleic Acids Res.* **2021**, *49*, 2985-2999.

[14] K. Kundert, J. E. Lucas, K. E. Watters, C. Fellmann, A. H. Ng, B. M. Heineike, C. M. Fitzsimmons, B. L. Oakes, J. Qu, N. Prasad, O. S. Rosenberg, D. F. Savage, H. El-Samad, J. A.Doudna, T. Kortemme, *Nat. Commun.* **2019**, *10*, 2127.

[15] R. S. Iwasaki, B. A. Ozdilek, A. D. Garst, A. Choudhury, R. T. Batey, *Nat. Commun.* **2020**, *11*, 1394.

[16] M. H. Hanewich-Hollatz, Z. Chen, L. M. Hochrein, J. Huang, N. A. Pierce, *ACS Cent. Sci.* **2019**, *5*, 1241-1249.

[17] L. M. Hochrein, H. Li, N. A. Pierce, *ACS Synth. Biol.* **2021**, *10*, 964-971.

[18] K.-H. Siu, W. Chen, *Nat. Chem. Biol.* **2019**, *15*, 217-220.

[19] E. M. Zhao, A. S. Mao, H. de Puig, K. Zhang, N. D. Tippens, X. Tan, F. A. Ran, I. Han, P. Q. Nguyen, E. J. Chory, T. Y. Hua, P. Ramesh, D. B. Thompson; C.Y. Oh, E. S. Zigon, M. A. English, J. J. Collins, *Nat. Biotechnol.* **2022**, *40*, 539-545.

[20] F. C. Simmel, B. Yurke, H. R. Singh, *Chem. Rev.* **2019**, *119*, 6326-6369.

[21] N. Xie, M. Li, Y. Wang, H. Lv, J. Shi, J. Li, Q. Li, F. Wang, C. Fan, *J. Am. Chem. Soc.* **2022**, *144*, 9479-9488.

[22] J. Deng, A. Walther, *J. Am. Chem. Soc.* **2020**, *142*, 21102-21109.

[23] L. Yue, S. Wang, Z. Zhou, I. Willner, *J. Am. Chem. Soc.* **2020**, *142*, 21577-21594.

[24] Z. Li, J. Wang, I. Willner, *Adv. Funct. Mater.* **2022**, *32*, 2200799.

[25] Z. Zhou, Y. Ouyang, J. Wang, I. Willner, *J. Am. Chem. Soc.* **2021**, *143*, 5071-5079.

[26] L. Qian, E. Winfree, *Science* **2011**, *332*, 1196-1201.

[27] D. Y. Zhang, G. Seelig, *Nat. Chem.* **2011**, *3*, 103-113.

[28] K. E. Bujold, A. Lacroix, H. F. Sleiman, *Chem* **2018**, *4*, 495-521.

[29] S. Lu, J. Shen, C. Fan, Q. Li, X. Yang, *Adv. Sci.* **2021**, *8*, 2100328.

[30] X. Liu, C.-H. Lu, I. Willner, *Acc. Chem. Res.* **2014**, *47*, 1673-1680.

[31] Y. Dai, A. Furst, C. C. Liu, *Trends Biotechnol.* **2019**, *37*, 1367-1382.

[32] J. K. Jung, C. M. Archuleta, K. K. Alam, J. B. Lucks, *Nat. Chem. Biol.* **2022**, *18*, 385-393.

[33] Y. Xiao, B. D. Piorek, K. W. Plaxco, A. J. Heeger, *J. Am. Chem. Soc.* **2005**, *127*, 17990-17991.

[34] A. Amodio, B. Zhao, A. Porchetta, A. Idili, M. Castronovo, C. Fan, F. Ricci, *J. Am. Chem. Soc.* **2014**, *136*, 16469-16472.

[35] T. Wang, H. Hellmer, F. C. Simmel, *Curr. Opin. Biotechnol.* **2023**, *79*, 102867.

[36] L. Oesinghaus, F. C. Simmel, *Nat. Commun.* **2019**, *10*, 2092.

[37] M. Jin, N. Garreau de Loubresse, Y. Kim, J. Kim, P. Yin, *ACS Synth. Biol.* **2019**, *8*, 1583-1589.

[38] R. Galizi, J. N. Duncan, W. Rostain, C. M. Quinn, M. Storch, M. Kushwaha, A. Jaramillo, *CRISPR J.* **2020**, *3*, 398-408.

[39] Y. Li, X. Teng, K. Zhang, R. Deng, J. Li, *Anal. Chem.* **2019**, *91*, 3989-3996.

[40] S. Gong, S. Zhang, X. Wang, J. Li, W. Pan, N. Li, B. Tang, *Anal. Chem.* **2021**, *93*, 15216-15223.

[41] T. Zhang, R. Deng, Y. Wang, C. Wu, K. Zhang, C. Wang, N. Gong, R. Ledesma-Amaro, X. Teng, C. Yang, T. Xue, Y. Zhang, Y. Hu, Q. He, W. Li, J. Li, *Nat. Biomed. Eng.* **2022**, *6*, 957-967.

[42] S. Peng, Z. Tan, S. Chen, C. Lei, Z. Nie, Chem. Sci. 2020, 11, 7362-7368.

[43] W. Feng, A. M. Newbigging, J. Tao, Y. Cao, H. Peng, C. Le, J. Wu, B. Pang, J. Li, D. L. Tyrrell, H. Zhang, X. C. Le, Chem. Sci. 2021, 12, 4683-4698.

[44] Y. Xiong, J. Zhang, Z. Yang, Q. Mou, Y. Ma, Y. Xiong, Y. Lu, *J. Am. Chem. Soc.* **2019**, *142*, 207-213.

[45] G. Rosati, A. Idili, C. Parolo, C. Fuentes-Chust, E. Calucho, L. Hu, C. d. C. Castro e Silva, L. Rivas, E. P. Nguyen, J. F. Bergua, R. Alvárez-Diduk, J. Muñoz, C. Junot, O. Penon, D. Monferrer, E. Delamarche, A. Merkoçi, *ACS Nano* **2021**, *15*, 17137-17149.

[46] A. A. Green, P. A. Silver, J. J. Collins, P. Yin, *Cell* **2014**, *159*, 925-939.

[47] Y. Hao, J. Li, Q. Li, L. Zhang, J. Shi, X. Zhang, A. Aldalbahi, L. Wang, C. Fan, F. Wang, *Angew. Chem. Int. Ed.* **2020**, *59*, 20612-20618.

[48] A. A. Green, *Emerg. Top. Life Sci.* **2019**, *3*, 507-516.

[49] R. T. Leenay, C. L. Beisel, *J. Mol. Biol.* **2017**, *429*, 177-191.

[50] F. J. Mojica, C. Díez-Villaseñor, J. García-Martínez, C. Almendros, *Microbiol.* **2009**, *155*, 733-740.

[51] Y. Wu, W. Luo, Z. Weng, Y. Guo, H. Yu, R. Zhao, L. Zhang, J. Zhao, D. Bai, X. Zhou, *Nucleic Acids Res.* **2022**, *50*, 11727-11737.

[52] W. Zhang, Y. Mu, K. Dong, L. Zhang, B. Yan, H. Hu, Y. Liao, R. Zhao, W. Shu, Z. Ye, Y. Lu, C. Wan, Q. Sun, L. Li, H. Wang, X. Xiao, Nucleic Acids Res. 2022, 50, 12674-12688.

[53] S. Chen, R. Wang, S. Peng, S. Xie, C. Lei, Y. Huang, Z. Nie, Chem. Sci. 2022, 13, 2011-2020.

[54] L. Gao, D. B. Cox, W. X. Yan, J. C. Manteiga, M. W. Schneider, T. Yamano, H. Nishimasu, O. Nureki, N. Crosetto, F. Zhang, *Nat. Biotechnol.* **2017**, *35*, 789-792.

[55] B. Zetsche, J. S. Gootenberg, O. O. Abudayyeh, I. M. Slaymaker, K. S. Makarova, P. Essletzbichler, S. E. Volz, J. Joung, J. Van Der Oost, A. Regev, E. V. Koonin, F. Zhang, *Cell* **2015**, *163*, 759-771.

[56] J. S. Chen, E. Ma, L. B. Harrington, M. Da Costa, X. Tian, J. M. Palefsky, J. A. Doudna, *Science* **2018**, *360*, 436-439.

[57] S. Ranallo, D. Sorrentino, F. Ricci, *Nat. Commun.* **2019**, *10*, 5509.

[58] F. Li, H. Zhang, Z. Wang, X. Li, X.-F. Li, X. C. Le, *J. Am. Chem. Soc.* **2013**, *135*, 2443-2446.

[59] F. Li, Y. Tang, S. M. Traynor, X.-F. Li, X. C. Le, *Anal. Chem.* **2016**, *88*, 8152-8157.

[60] M. Rossetti, R. Merlo, N. Bagheri, D. Moscone, A. Valenti, A. Saha, P. R. Arantes, R. Ippodrino, F. Ricci, I. Treglia, E. Delibato, J. Van der Oost, G. Palermo, G. Perugino, A. Porchetta, *Nucleic Acids Res.* **2022**, *50*, 8377-8391.

[61] T. Yamano, B. Zetsche, R. Ishitani, F. Zhang, H. Nishimasu, O. Nureki, *Mol. Cell* **2017**, *67*, 633-645.

[62] R. T. Fuchs, J. Curcuru, M. Mabuchi, P. Yourik, G. B. Robb, *BioRxiv* **2019**, 600890.

[63] A. Saha, P. R. Arantes, R. V. Hsu, Y. B. Narkhede, M. Jinek, G. Palermo, *J. Chem. Inf. Model.* **2020**, *60*, 6427-6437.

[64] D. C. Swarts, M. Jinek, *Mol. Cell* **2019**, *73*, 589-600. e584.

[65] S. Bracaglia, S. Ranallo, F. Ricci, *Angew. Chem. Int. Ed.* **2023**, *62*, e202216512.

[66] R. P. Chen, D. Blackstock, Q. Sun, W. Chen, *Nat. Chem.* **2018**, *10*, 474-481.

[67] H. J. van der Veer, E. A. van Aalen, C. M. Michielsen, E. T. Hanckmann, J. Deckers, M. M. van Borren, J. Flipse, A. J. Loonen, J. P. Schoeber, M. Merkx, *ACS Cent. Sci.* **2023**, *9*, 657-667.

[68] T. Azad, A. Tashakor, S. Hosseinkhani, *Anal. Bioanal. Chem.* **2014**, *406*, 5541-5560.

[69] M. Rossetti, A. Bertucci, T. Patiño, L. Baranda, A. Porchetta, *Chem. Eur. J.* **2020**, *26*, 9826-9834.

[70] A. Porchetta, R. Ippodrino, B. Marini, A. Caruso, F. Caccuri, F. Ricci, *J. Am. Chem. Soc.* **2018**, *140*, 947-953.

[71] M. Rossetti, S. Brannetti, M. Mocenigo, B. Marini, R. Ippodrino, A. Porchetta, *Angew. Chem.* **2020**, *132*, 15083-15088.

[72] K. Tenda, B. van Gerven, R. Arts, Y. Hiruta, M. Merkx, D. Citterio, *Angew. Chem. Int. Ed.* **2018**, *57*, 15369-15373.

[73] M. Neri, J. Kang, J. M. Zuidema, J. Gasparello, A. Finotti, R. Gambari, M. J. Sailor, A. Bertucci, R. Corradini, *ACS Biomater. Sci. Eng.* **2021**, *8*, 4123-4131.

[74] A. Bertucci, A. Manicardi, R. Corradini, *Detection of non-amplified Genomic DNA* **2012**, 89-124.

[75] D. Fleury, S. A. Wharton, J. J. Skehel, M. Knossow, T. Bizebard, *Nat. Struct. Biol.* **1998**, *5*, 119-123.

[76] S. Wang, L. You, M. Dai, Y. Zhao, *J. Cell. Mol. Med.* **2020**, *24*, 10279-10289.

[77] S. Bracaglia, S. Ranallo, K. W. Plaxco, F. Ricci, *ACS Sens.* **2021**, *6*, 2442-2448.

TOC

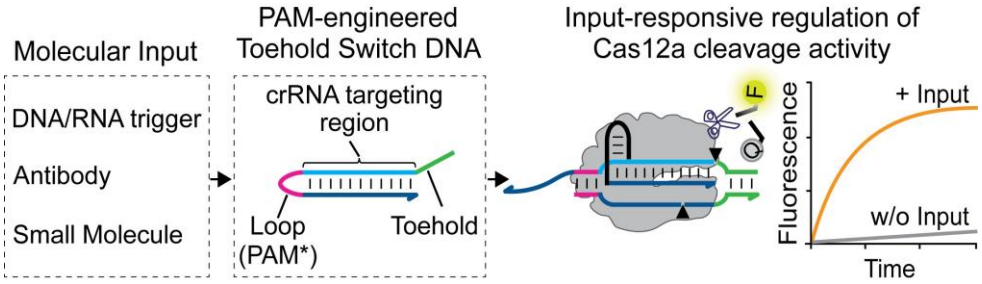
Molecular Input
DNA/RNA trigger
Antibody
Small Molecule
PAM-engineered
Toehold Switch DNA
crRNA targeting
region
Loop
(PAM*)
Toehold
Input-responsive regulation of
Cas12a cleavage activity
F
Q
Fluorescence
+ Input
w/o Input
Time